Taiwanese Journal of Obstetrics & Gynecology 56 (2017) 210–216

Contents lists available at ScienceDirect

Taiwanese Journal of Obstetrics & Gynecology

journal homepage: www.tjog-online.com

Original Article

Gene set-based analysis of mucinous ovarian carcinoma

Chia-Ming Chang [a, b, c], Peng-Hui Wang [a, c, d, e], Huann-Cheng Horng [a, c, *]

[a] Department of Obstetrics and Gynecology, Taipei Veterans General Hospital, Taipei, Taiwan
[b] Institute of Oral Biology, National Yang-Ming University, Taipei, Taiwan
[c] Department of Obstetrics and Gynecology, National Yang-Ming University, Taipei, Taiwan
[d] Institute of Clinical Medicine, National Yang-Ming University, Taipei, Taiwan
[e] Department of Medical Research, China Medical University Hospital, Taichung, Taiwan

ARTICLE INFO

Article history:
Accepted 27 December 2016

Keywords:
function
gene expression
mucinous ovarian carcinoma

ABSTRACT

Objective: Mucinous ovarian carcinoma (MOC) is an uncommon subtype of epithelial ovarian cancers, and the pathogenesis is still poorly understood because of its rarity. We conducted a gene set-based analysis to investigate the pathogenesis of MOC by integrating microarray gene expression datasets based on the regularity of functions defined by gene ontology or canonical pathway databases.

Materials and methods: Forty-five pairs of MOC and normal ovarian tissue sample gene expression profiles were downloaded from the National Center for Biotechnology Information Gene Expression Omnibus database. The gene expression profiles were converted to the gene set regularity indexes by measuring the change of gene expression ordering in a gene set. Then the pathogenesis of MOC was investigated with the differences of function regularity with the gene set regularity indexes between the MOC and normal control samples.

Results: The informativeness of the gene set regularity indexes was sufficient for machine learning to accurately recognize and classify the functional regulation patterns with an accuracy of 99.44%. The statistical analysis revealed that the GTPase regulators and receptor tyrosine kinase erbB-2 (ERBB2) were the most important aberrations; the exploratory factor analysis revealed phosphoinositide 3-kinase-activating kinase, G-protein coupled receptor pathway, oxidoreductase activity, immune response, peptidase activity, regulation of translation, and transport and channel activity were also involved in the pathogenesis of MOC.

Conclusion: Investigating the pathogenesis of MOC with the functionome provided a comprehensive view of the deregulated functions of this disease. In addition to GTPase regulators and ERBB2, a plenty of deregulated functions such as phosphoinositide 3-kinase, G-protein coupled receptor pathway, and immune response also participated in the interaction network of MOC pathogenesis.

Introduction

Primary mucinous ovarian carcinoma (MOC) is an uncommon subtype of epithelial ovarian cancers, accounting for 3–4% of all ovarian carcinomas [1,2]. Currently, the carcinogenesis of MOC is still poorly understood because of its rarity. Two genetic aberrations, KRAS and receptor tyrosine kinase erbB-2 (ERBB2), are known to be involved in the pathogenesis of MOC [3]; besides, knowledge about the function regulation and pathogenesis of this cancer is limited. Microarray gene expression [4–6] is the primary tool of investigation of the pathogenesis of complex diseases such as mucinous ovarian cancer. To further understand the pathogenesis of MOC, we conducted an integrative analysis of mucinous ovarian cancer with the microarray gene expression datasets downloaded from publicly available databases.

The workflow of this gene set-based analysis was introduced before [7–10]. In brief, it consisted of two steps. First, microarray gene expressions were converted to a gene set regularity (GSR) index by computing the expression ordering change among genes in a given gene set defined by the gene ontology (GO) or the canonical pathway database downloaded from the Molecular Signature Database [11]. Each gene set contains a group of genes, defining biological process, molecular function, or cellular component; for simplification, we called them “function” in this

* Corresponding author. Department of Obstetrics and Gynecology, Taipei Veterans General Hospital and National Yang-Ming University, 201, Section 2, Shih-Pai Road, Taipei 112, Taiwan.
E-mail address: hchorng@vghtpe.gov.tw (H.-C. Horng).

http://dx.doi.org/10.1016/j.tjog.2016.12.016

study. By measuring the change of gene expression level orderings between cancerous and normal states, regularity of the function defined by that gene set could be quantified. In the second step, the pathogenesis of MOC was investigated with the 1454 GO term- or 1330 canonical pathway-defined functions. We utilized exploratory factor analysis (EFA) to discover important deregulated functions and the interaction network involved in the pathogenesis of MOC.

Materials and methods

Microarray datasets, gene set definition, and data processing

We downloaded gene expression microarray datasets in the SOFT format from the National Center for Biotechnology Information Gene Expression Omnibus database. MOC and normal ovarian tissue were used for comparison. The common genes among all the datasets and the associated gene expression data were included. Datasets and gene sets were discarded if the number of the common genes and gene elements was less than 8000 and 3, respectively.

Computing GSR indexes

Figure 1 shows the workflow for computing the GSR indexes, which was modified from the Differential Rank Conservation [12]. The Differential Rank Conservation is designed to measure the perturbation of a given gene set by quantifying the change of gene expression orderings of gene elements in that gene set. Instead of measuring the perturbation, the GSR index quantifies the change of gene expression orderings between two phenotypes in a gene set. For this purpose, the GSR indexes of the MOC and normal ovarian tissue groups were computed by comparing the sample's gene expression orderings with the baseline gene set ordering template, defined as the most common gene expression ordering in a gene set among all the normal ovarian tissue samples. Subsequent analyses of MOC and normal ovarian tissue GSR indexes were carried out based on this baseline. The baseline gene set ordering template for each gene set was established by pairwise comparison between the expression levels of two genes for all possible combinations of gene pair. Establishment of the baseline gene set expression ordering template and computation of the GSR indexes were executed in R environment. The code and test datasets can be obtained from the GitHub (https://github.com/carlzang/GSR-model.git).

Statistical analysis

We used Mann–Whitney *U* test to test the differences between the MOC and control GSR indexes, and the data were corrected by

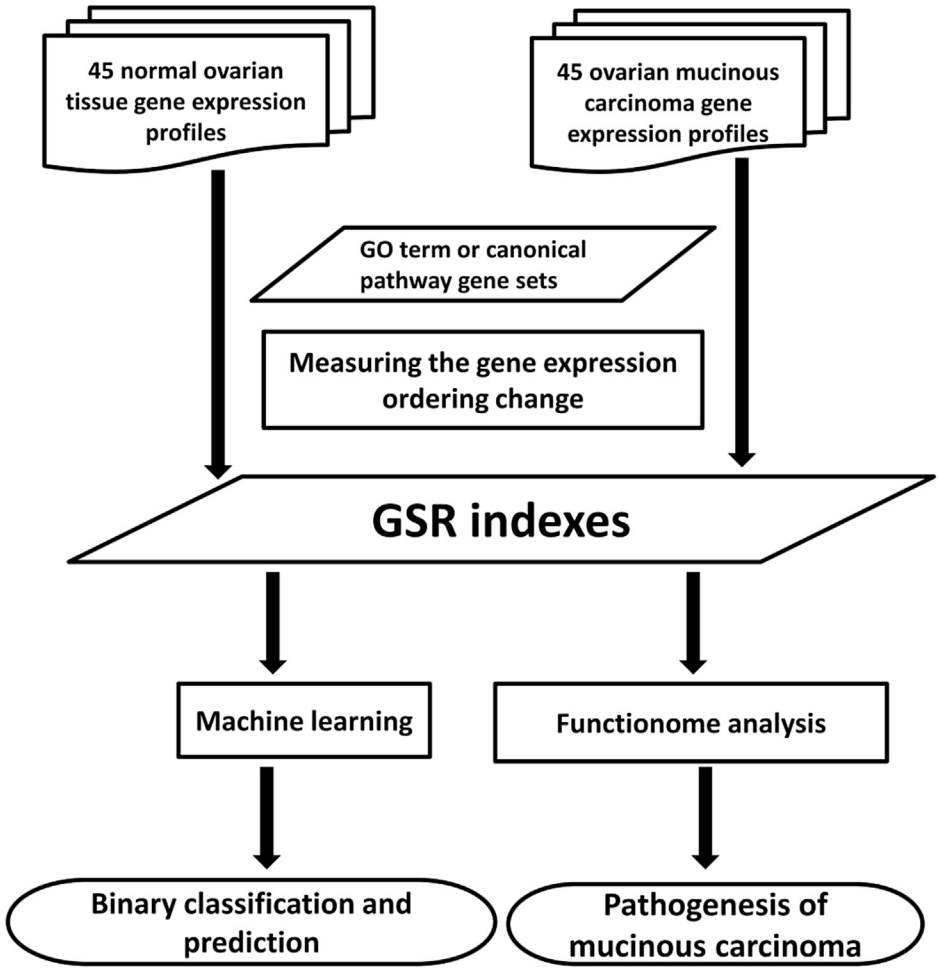

Figure 1. Workflow of the GSR model. The MOC or control GSR index was computed by converting the gene expression orderings of MOC or normal ovarian control sample through each GO term or canonical pathway gene set. Machine learning algorithm was trained to recognize the patterns consisting of the GSR indexes and then execute the binary (case–control) classifications. Functionome analysis was carried out to investigate the pathogenesis of MOC. GO = gene ontology; GSR = gene set regularity; MOC = mucinous ovarian carcinoma.

multiple hypotheses using the false discovery rate (Benjamini–Hochberg procedure). The significance was defined for $p < 0.001$.

Classification and prediction of datasets by machine learning

Matrices of the GSR index computed through the GO term and canonical pathway gene sets were classified and predicted by machine learning support vector machines (SVMs) with "kernlab" [13], which is an R package for kernel-based machine learning methods and is used to classify patterns of the GSR indexes with the setting of kernel = "vanilladot" (linear kernel function). The performance of classification and prediction by SVMs was measured by five-fold cross validation with the cumulative results of 10 consecutive classifications. The performance was assessed with the sensitivity, specificity, as well as accuracy and area under the curve. The area under the curve was computed by an R package "pROC" [14].

EFA for deregulated GO terms and establishment of the GO tree

The deregulated GO terms of $p < 0.001$ were selected for EFA. EFA was executed with the R package "psych" (version 1.5.8). The number of factors to be extracted was determined by the function "pa.parellel." The factoring method used in this study was set to "pa" and the correlation matrix rotation method was "promax."

The tree of the deregulated GO terms was constructed by the "RamiGO" [15], an R package providing functions to interact with the AmiGO 2 web server and retrieving GO trees.

Construction of interaction network

The network was established with the mutual information based on entropy estimates from k-nearest neighbor distances and Algorithm for the Reconstruction of Accurate Cellular Networks for the reconstruction of interaction networks (multiplicative model) using the R package "parmigene" (version 1.0.2). The network was output in .gml format and displayed on Cytoscape (version 3.3.0).

Results

Sample information and means of the GSR indexes of MOC

DNA microarray gene expression datasets were downloaded from the National Center for Biotechnology Information Gene Expression Omnibus database, including 45 MOC and 45 normal ovarian tissue control samples. The microarray gene expression dataset series of MOC utilized in this study were GSE20565, GSE26193, GSE30161, GSE44104, GSE51088, GSE55512, and GSE6008, containing three microarray platforms including GPL570, GPL7264, and GPL96. The GSR indexes ranged from 0 to 1; 0 represented the most chaotic function regularity, while 1 represented the gene expression level orderings in the MOC group that were completely identical to the most common gene expression level orderings in the normal control population. Table 1 shows the means of the GSR indexes computed through GO terms. The MOC group had smaller GSR levels than the normal control group, and the difference was statistically significant at $p < 0.0001$. Distribution of the GSR indexes for the MOC and control groups was displayed on the histogram. As Figure 2 shows, a group of GSR indexes with worse GSR was observed on the left side with the peak at 0.5. It indicated that a population of deregulated GO term-defined functions existed in the MOC group.

Functional regulation patterns classified and predicted by machine learning

Machine learning can learn from data by building a model and recognizing patterns to make prediction or decisions. We trained SVM [16], a high-performance machine learning algorithm to classify and predict between the MOC and the normal control datasets with their functional regulation patterns consisting of the GSR index matrices. As Table 1 shows, accuracies of binary classification (MOC vs. control) were 98.33%, 99.44%, and 98.89% when computing, respectively, through the GO term, canonical pathway gene sets, and a combination of both. This result revealed that the informativeness of the GSR indexes was sufficient for SVMs to undergo accurate classification and prediction.

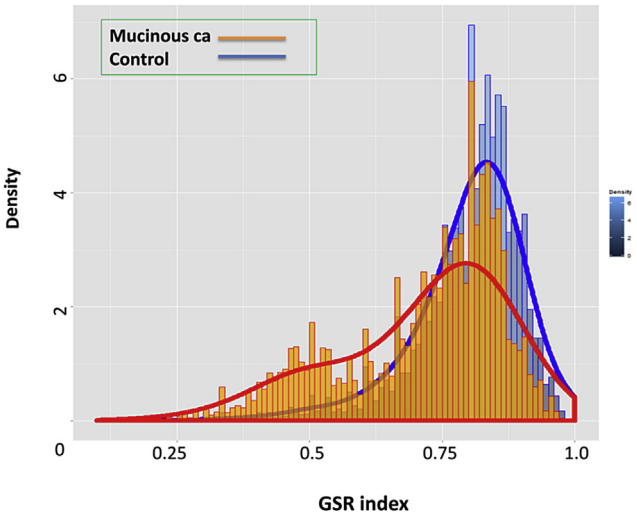

Figure 2. Distribution of the GSR indexes for the MOC (orange) and control groups (blue). The MOC group had smaller GSR index levels in comparison with the normal control group. A group of GSR indexes with smaller GSR index levels on the left side of the histogram was observed, indicating a population of deregulated functions in the pathogenesis of MOC. ca = carcinoma; GO = gene ontology; GSR = gene set regularity; MOC = mucinous ovarian carcinoma. (For interpretation of the references to colour in this figure legend, the reader is referred to the web version of this article.)

Table 1
Means and SDs of the MOC and control groups, and performance of the binary (MOC vs. control group) classification and prediction by SVMs with the GSR indexes computed through the GO terms, canonical pathways, or combination of both (GO terms + canonical pathways).

Gene set database	MOC Mean (SD)	Control Mean (SD)	Sensitivity (SD)	Specificity (SD)	Accuracy (SD)	AUC
GO terms	0.7252 (0.1481)	0.7633 (0.1353)	0.9889 (0.0351)	0.9766 (0.0507)	0.9833 (0.02683)	0.9840
Canonical pathways	0.7327 (0.1482)	0.7671 (0.1354)	0.9889 (0.0351)	1.0000 (0.0000)	0.9944 (0.0175)	0.9945
GO terms + canonical pathways	0.7288 (0.1482)	0.7651 (0.1354)	0.9916 (0.0263)	0.9875 (0.0395)	0.9889 (0.0234)	0.9890

Sensitivities, specificities, accuracies, SDs, and AUC were assessed by five-fold cross validation. Each measurement was computed by the cumulative results of 10 consecutive classifications and predictions.
AUC = area under the curve; GO = gene ontology; MOC = mucinous ovarian carcinoma; SD = standard deviation; SVM = support vector machine.

Most deregulated functions of MOC

Table 2 displays the top 50 most deregulated GO terms ranked by the *p* values. The first deregulated GO term was "aldo keto reductase activity" (GO:0004033), followed by "vitamin transport" (GO:0051180) and "Rho guanyl nucleotide exchange factor activity" (GO:0005089). "Aldo keto reductase activity" is a child GO term of "oxidoreductase activity"; besides, the "oxidoreductase activity GO 0016616" (39th) and "oxidoreductase activity acting on CH OH group of donors" (41th) in Table 2 were also GO terms related to oxidative stress. In addition to "vitamin transport," there were many deregulated functions related to transport, including the "cofactor transport" (14th), "ion transport" (36th) and "di–tri-valent inorganic cation transport" (49th) in Table 2. "Rho guanyl nucleotide exchange factor activity," "guanyl nucleotide exchange factor activity" (35th), and "Ras guanyl nucleotide exchange factor activity" (48th) are the GTPase regulator responses to RAS activation and signaling. The deregulated GO terms in the table could be summarized to the following categories: guanyl nucleotide exchange factor activity, binding, transport, channel activity, oxidoreductase activity, metabolism, immune response, phosphoinositide 3-kinase (PI3K) signaling, and protein tyrosine kinase activity.

Table 3 displays the top 50 deregulated canonical pathways ranked by the *p* values. The first deregulated canonical pathway was "Reactome organic cation anion zwitterion transport," followed by "Reactome downregulation of ERBB2 ErbB3 signaling". The third deregulated pathway "Reactome olfactory signaling pathway" was probably a false positivity because it contained many gene set elements related to G-protein, an important deregulated function appeared in MOC detected by the GSR model. The sixth deregulated pathway "Reactome PI3K events in ERBB2 signaling" indicated the possible interaction between the ErbB and PI3K played in the pathogenesis of MOC.

Table 2
Top 50 most deregulated GO terms for mucinous ovarian cancers ranked by *p* values.

	Deregulated GO terms	*p*
1	Aldo keto reductase activity	7.84E−15
2	Vitamin transport	5.58E−14
3	Rho guanyl nucleotide exchange factor activity	4.79E−12
4	Small conjugating protein binding	5.44E−12
5	Ubiquitin binding	5.44E−12
6	Calcium channel activity	5.49E−12
7	Negative regulation of immune system process	8.57E−12
8	Carbohydrate biosynthetic process	1.45E−11
9	Inositol or phosphatidylinositol phosphatase activity	1.94E−11
10	Neuropeptide binding	2.99E−11
11	Neuropeptide receptor activity	2.99E−11
12	Transmembrane receptor protein tyrosine kinase activity	2.99E−11
13	Innate immune response	3.15E−11
14	Cofactor transporter activity	4.11E−11
15	Sulfotransferase activity	4.34E−11
16	Ligand-gated channel activity	4.41E−11
17	Neuropeptide signaling pathway	4.41E−11
18	Sarcomere	1.35E−10
19	Chloride channel activity	1.35E−10
20	Oxygen and reactive oxygen species metabolic process	1.40E−10
21	Ion channel activity	1.53E−10
22	Protein tyrosine kinase activity	1.65E−10
23	Substrate-specific channel activity	2.19E−10
24	Chaperone binding	2.67E−10
25	Acetylcholine binding	3.34E−10
26	Synaptic transmission	3.34E−10
27	Negative regulation of cytoskeleton organization and biogenesis	3.42E−10
28	Steroid binding	3.64E−10
29	Anion channel activity	6.17E−10
30	Humoral immune response	6.17E−10
31	Organic anion transmembrane transporter activity	6.49E−10
32	Regulation of immune effector process	7.35E−10
33	Sterol binding	7.40E−10
34	Cation channel activity	8.94E−10
35	Guanyl nucleotide exchange factor activity	8.94E−10
36	Ion transport	8.94E−10
37	Myofibril	9.24E−10
38	Transmission of nerve impulse	9.91E−10
39	Oxidoreductase activity GO 0016616	1.01E−09
40	Neurotransmitter binding	1.13E−09
41	Oxidoreductase activity acting on CH OH group of donors	1.15E−09
42	Aromatic compound metabolic process	1.52E−09
43	Regulation of viral reproduction	1.55E−09
44	Actin filament-based movement	1.62E−09
45	Transferase activity transferring sulfur-containing groups	2.05E−09
46	Intercalated disc	2.08E−09
47	Developmental maturation	2.79E−09
48	RAS guanyl nucleotide exchange factor activity	2.79E−09
49	Di–tri-valent inorganic cation transport	2.90E−09
50	Calcium ion transport	3.07E−09

GO = gene ontology.

Table 3
Top 50 deregulated canonical pathways for MOC ranked by *p* values.

	Deregulated canonical pathways	*p*
1	Reactome organic cation anion zwitterion transport	1.34E−15
2	Reactome downregulation of ERBB2 ERBB3 signaling	2.25E−15
3	Reactome olfactory signaling pathway	2.62E−12
4	PID integrin 5 pathway	3.47E−12
5	Reactome digestion of dietary carbohydrate	1.21E−11
6	Reactome PI3K events in ERBB2 signaling	2.93E−11
7	BioCarta MTA3 pathway	2.96E−11
8	Reactome regulation of insulin-like growth factor (IGF) activity by insulin-like growth factor-binding proteins (IGFBPs)	4.49E−11
9	Reactome regulated proteolysis of p75NTR	6.46E−11
10	KEGG glycosphingolipid biosynthesis ganglio series	6.67E−11
11	Reactome activated AMPK stimulates fatty acid oxidation in muscle	1.68E−10
12	Reactome Nef-mediated downregulation of MHC class I complex cell surface expression	3.13E−10
13	Reactome peptide ligand-binding receptors	3.20E−10
14	Reactome class A1 rhodopsin-like receptors	5.92E−10
15	Reactome intrinsic pathway	5.92E−10
16	KEGG butanoate metabolism	7.85E−10
17	BioCarta RAC1 pathway	8.02E−10
18	KEGG olfactory transduction	9.56E−10
19	Reactome CD28-dependent PI3K Akt signaling	9.56E−10
20	Reactome endogenous sterols	9.56E−10
21	KEGG phosphatidylinositol signaling system	1.22E−09
22	KEGG glycerolipid metabolism	1.28E−09
23	KEGG inositol phosphate metabolism	1.28E−09
24	Reactome formation of fibrin clot clotting cascade	1.28E−09
25	Reactome interaction between L1 and ankyrins	1.28E−09
26	Reactome norepinephrine neurotransmitter release cycle	1.28E−09
27	KEGG neuroactive ligand receptor interaction	1.54E−09
28	KEGG steroid hormone biosynthesis	2.06E−09
29	Reactome apoptotic cleavage of cell adhesion proteins	2.13E−09
30	Reactome post-chaperonin tubulin folding pathway	2.13E−09
31	Reactome signaling by RoBo receptor	2.34E−09
32	Reactome PI3K cascade	2.77E−09
33	KEGG fructose and mannose metabolism	2.94E−09
34	KEGG glyoxylate and dicarboxylate metabolism	2.98E−09
35	Reactome GABA synthesis release reuptake and degradation	2.98E−09
36	Reactome muscle contraction	2.98E−09
37	Reactome striated muscle contraction	2.98E−09
38	KEGG tryptophan metabolism	3.52E−09
39	Reactome negative regulation of the PI3K Akt network	4.21E−09
40	Reactome regulation of gene expression in beta cells	4.53E−09
41	BioCarta lectin pathway	4.69E−09
42	Reactome GPCR ligand binding	4.69E−09
43	Reactome activated NOTCH1 transmits signal to the nucleus	5.38E−09
44	Reactome cytochrome P450 arranged by substrate type	5.38E−09
45	Reactome unblocking of NMDA receptor glutamate binding and activation	5.84E−09
46	KEGG fatty acid metabolism	6.29E−09
47	Reactome signaling by ERBB4	8.48E−09
48	Reactome energy-dependent regulation of mTOR by LKB1 AMPK	8.85E−09
49	KEGG ascorbate and aldarate metabolism	1.24E−08
50	Naba ECM regulators	1.26E−08

GPCR = G-protein coupled receptor pathway; MOC = mucinous ovarian carcinoma; PI3K = phosphoinositide 3-kinase; PID = Pathway Interaction Database; MTA3 = metastasis associated 1 family member 3; p75NTR = p75 neurotrophin receptor; KEGG = Kyoto Encyclopedia of Genes and Genomes; AMPK = 5' adenosine monophosphate-activated protein kinase; RAC1 = Ras-related C3 botulinum toxin substrate 1; MHC = major histocompatibility complex; NOTCH1 = notch homolog 1, translocation-associated; NMDA = N-methyl-D-aspartate; mTOR = mechanistic target of rapamycin; LKB1, liver kinase B1; ECM, extracellular matrix.

EFA, establishment of deregulated GO tree, and interactive network of deregulated functions of MOC

Numerous significantly deregulated GO terms were involved in the pathogenesis, as Table 2 shows. EFA can discover the elements of underlying interactive network among a large number of variables, so we utilized it to disclose the networks involved in the pathogenesis of MOC. The EFA detected three groups of deregulated functions, containing 342 gene set elements in total. To reduce the redundancy and summarize these elements, these GO terms were merged and mapped to the GO trees according to their GO hierarchy. Figure 3 shows the screenshot of the full deregulated GO tree of MOC and important deregulated GO terms. The deregulated GO terms in the table could be summarized to the following categories: response to stress, system development, cytoskeleton organization, chromosome organization, G-protein coupled receptor pathway, immune response, cytokine receptor activity, regulation of cell cycle, cell–cell signaling, protein binding, DNA binding, negative regulation of cytokine biosynthesis process, negative regulation of translation, GTPase regulator activity, oxidoreductase activity, peptidase activity, protein kinase activity, and transmembrane transporter activity. The interaction network of deregulated functions reconstructed based on the mutual information is displayed in Figure 4. As a complex disease, MOC exhibited numerous deregulated functions; they affected each other and formed the pathogenesis network of MOC.

Discussion

This study investigated the pathogenesis of MOC with the quantified functions represented by the GSR indexes. Our results demonstrated that the GSR indexes might provide sufficient

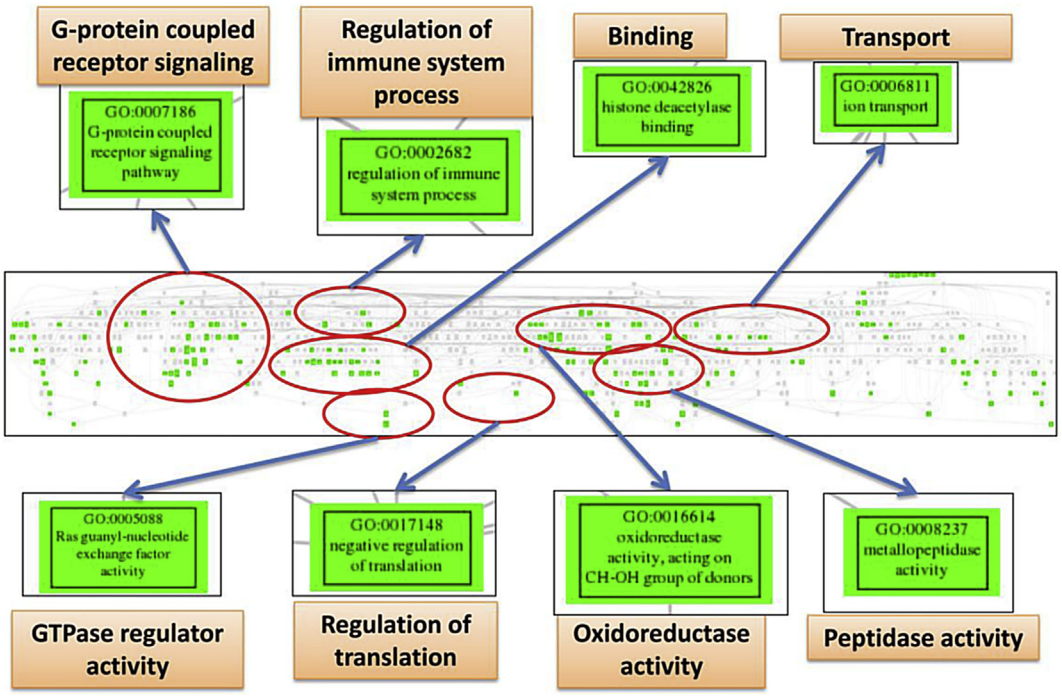

Figure 3. Screenshot of the full MOC GO tree (middle). The important elements (green boxes) in the cluster of deregulated GO terms were magnified to view the details and labeled by their common parental GO terms (orange rectangles). GO = gene ontology; GSR = gene set regularity; MOC = mucinous ovarian carcinoma. (For interpretation of the references to colour in this figure legend, the reader is referred to the web version of this article.)

information for accurate pattern recognition by machine learning. This gene set-based analysis revealed plenty of deregulated functions as well as their interactions involved in the pathogenesis of MOC.

KRAS and ERBB2 were well-known genetic aberrations participating in the carcinogenesis of MOC [3]. KRAS is a GTPase that can turn on downstream effectors such as PI3K by binding to GTP activated by GTPase-activating proteins, or be turned off by

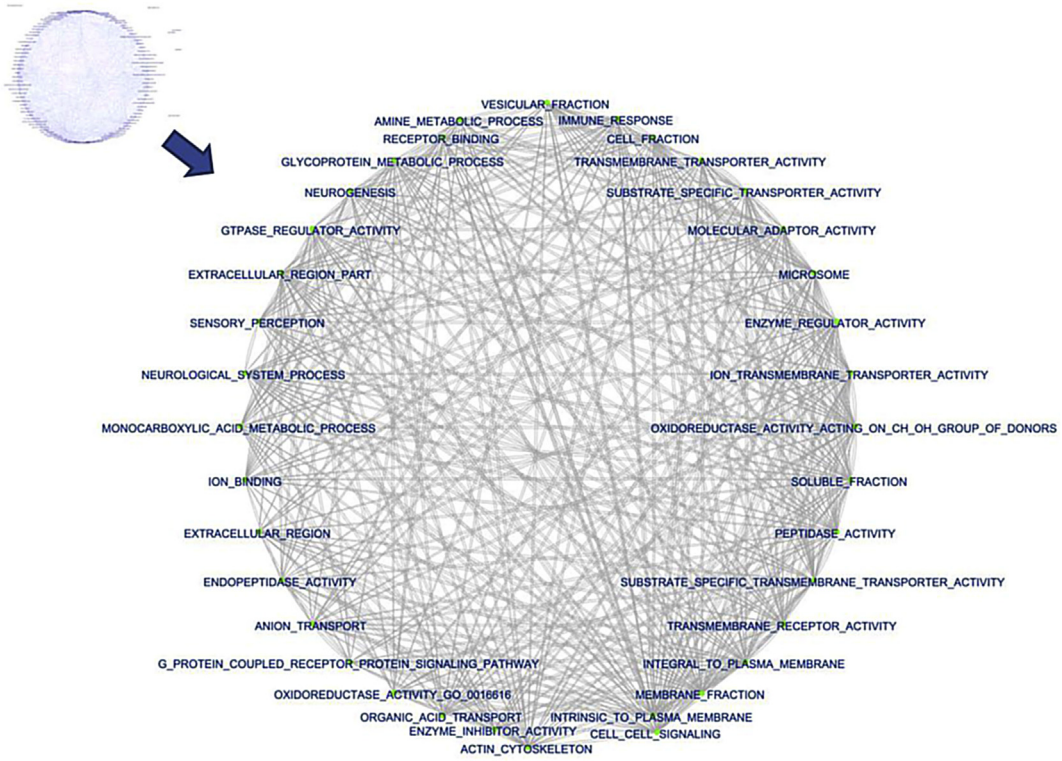

Figure 4. Interactive network reconstructed by the GO term elements from EFA. Only the nodes with degrees more than 40 are shown in detail. EFA = exploratory factor analysis; GO = gene ontology.

conversion of guanosine diphosphate (GTP) to guanosine triphosphate (GDP) initiated by guanyl nucleotide exchange factors [17]. ERBB2 is a member of the human epidermal growth factor receptor family, consists of four receptor tyrosine kinases, can active PI3K or other signaling pathways, and results in deregulated cell cycle control [18]. Mackenzie and colleagues [19] using the Ion Torrent PGM platform found that concurrent ERBB2 amplification and KRAS mutation were observed in a substantial number of MOC cases, suggesting that the prevalence of RAS alteration and striking co-occurrence of pathway "double-hits" supports a critical role for tumor progression in the MOC.

GTPase regulators (Rho or Ras guanyl nucleotide exchange factors), ERBB2, and PI3K signaling were the most deregulated functions detected by the GSR model. The results of EFA further disclosed that the protein tyrosine kinase activity, G-protein coupled receptor pathway, oxidoreductase activity, cytokines, immune response, and chromosome organization were also involved in the pathogenesis of MOC, and the network in Figure 4 revealed the evidence of extensive interactions among these deregulated functions. The possible signaling cascade of MOC can be inferred from the findings in our study: ligands, such as growth factors and cytokines, bind to ERBB2 and initiate signaling downstream cascades, including RAS and PI3K. The activation or deactivation of RAS is switched by two conformational states regulated by GTPase-activating proteins or guanyl nucleotide exchange factors. In case of carcinogenesis of MOC, these GTPases were deregulated as a result of RAS mutation. PI3K, activated by deregulated RAS, converts phosphatidylinositol (4,5)-bisphosphate into phosphatidylinositol (3,4,5)-trisphosphate. Phosphatidylinositol (3,4,5)-trisphosphate, in turn, binds Akt and stimulates its kinase activity, and leads to deregulated cell growth and proliferation.

In this study, we investigated MOC with the functionome instead of the differentially expressed genes [20–24]. This approach has several advantages. First, biological functions are more easily understood than gene symbols, and second, conversion of tens of thousands of gene expressions to approximately 1000 gene set-defined functions will reduce the complexity and noise of data. Computation of the gene expression ranking in a gene set will also take the gene interactions in a gene set into consideration. However, the major limitation of this approach was false positivity, such as the third most deregulated canonical pathway "Reactome olfactory signaling pathway" in Table 3.

In conclusion, with the GSR indexes converted from the microarray gene expression profiles downloaded from the publicly available databases, the functionome analysis revealed the network of MOC pathogenesis: in addition to the most significant aberrations including GTPase regulator activity and ERBB2 signaling, plenty of deregulation functions as well as the interactions, including PI3K signaling, oxidoreductase activity, immune response, channel activity, G-protein coupled receptor pathway, protein tyrosine kinase, peptidase activity, regulation of translation, and transport, were also involved in the pathogenesis of MOC.

Conflicts of interest

The authors have no conflicts of interest relevant to this article.

Acknowledgments

This study was supported by grants from the Ministry of Science and Technology, Executive Yuan (MOST 103-2314-B-010-043-MY3), and Taipei Veterans General Hospital (V105C-096, V106C-129, V106D23-001-MY2-1, and V106A-012). We also appreciate the Clinical Research Core Laboratory and the Medical Science & Technology Building of Taipei Veterans General Hospital for providing experimental space and facilities.

References

[1] Chen CK, Lee MY, Lin WL, Wang YT, Han CP, Yu CP, et al. A qualitative study comparing the assay performance characteristics between the 2007 and the 2013 American Society for Clinical Oncology and College of American Pathologists HER2 scoring methods in mucinous epithelial ovarian cancer. Medicine (Baltimore) 2014;93:e171.
[2] Sung PL, Chang YH, Chao KC, Chuang CM, Task Force on Systematic Review and Meta-analysis of Ovarian Cancer. Global distribution pattern of histological subtypes of epithelial ovarian cancer: a database analysis and systematic review. Gynecol Oncol 2014;133:147–54.
[3] Ledermann JA, Luvero D, Shafer A, O'Connor D, Mangili G, Friedlander M, et al. Gynecologic Cancer InterGroup (GCIG) consensus review for mucinous ovarian carcinoma. Int J Gynecol Cancer 2014;24:S14–9.
[4] Perren TJ. Mucinous epithelial ovarian carcinoma. Ann Oncol 2016;27:i53–7.
[5] Luo JD, Chang YJ, Chang CM, You JF, Wei PL, Chiou CC. GeneGazer: a toolkit integrating two pipelines for personalized profiling and biosignature identification. Cancer Genomics Proteomics 2016;13:141–50.
[6] Lee YS, Hwang SG, Kim JK, Park TH, Kim YR, Myeong HS, et al. Topological network analysis of differentially expressed genes in cancer cells with acquired gefitinib resistance. Cancer Genomics Proteomics 2015;12:153–66.
[7] Shih CL, Luo JD, Chang JW, Chen TL, Chien YT, Yu CJ, et al. Circulating messenger RNA profiling with microarray and next-generation sequencing: cross-platform comparison. Cancer Genomics Proteomics 2015;12:223–30.
[8] Chang CM, Chiou SH, Yang MJ, Yen MS, Wang PH. Gene set-based integrative analysis of ovarian clear cell carcinoma. Taiwan J Obstet Gynecol 2016;55:552–7.
[9] Chang CM, Chuang CM, Wang ML, Yang MJ, Chang CC, Yen MS, et al. Gene set-based functionome analysis of pathogenesis in epithelial ovarian serous carcinoma and the molecular features in different FIGO stages. Int J Mol Sci 2016;17. pii:E886.
[10] Chang CM, Chuang CM, Wang ML, Yang YP, Chuang JH, Yang MJ, et al. Gene set-based integrative analysis revealing two distinct functional regulation patterns in four common subtypes of epithelial ovarian cancer. Int J Mol Sci 2016;17. pii:E1272.
[11] Subramanian A, Tamayo P, Mootha VK, Mukherjee S, Ebert BL, Gillette MA, et al. Gene set enrichment analysis: a knowledge-based approach for interpreting genome-wide expression profiles. Proc Natl Acad Sci U S A 2005;102:15545–50.
[12] Eddy JA, Hood L, Price ND, Geman D. Identifying tightly regulated and variably expressed networks by Differential Rank Conservation (DIRAC). PLoS Comput Biol 2010;6:e1000792.
[13] Karatzoglou A, Smola A, Hornik K. Kernel-based machine learning lab. Version 0.9-24. 2016. Available at: https://cran.r-project.org/web/packages/kernlab/kernlab.pdf. Accessed May, 1, 2016.
[14] Robin X, Turck N, Hainard A, Tiberti N, Lisacek F, Sanchez JC, et al. pROC: an open-source package for R and S+ to analyze and compare ROC curves. BMC Bioinformatics 2011;12:77.
[15] Schröder MS, Gusenleitner D, Quackenbush J, Culhane AC, Haibe-Kains B. RamiGO: an R/Bioconductor package providing an AmiGO visualize interface. Bioinformatics 2013;29:666–8.
[16] Cortes C, Vapnik V. Support-vector networks. Mach Learn 1995;20:273.
[17] Castellano E, Downward J. RAS interaction with PI3K: more than just another effector pathway. Genes Cancer 2011;2:261–74.
[18] Harari D, Yarden Y. Molecular mechanisms underlying ErbB2/HER2 action in breast cancer. Oncogene 2000;19:6102–14.
[19] Mackenzie R, Kommoss S, Winterhoff BJ, Kipp BR, Garcia JJ, Voss J, et al. Targeted deep sequencing of mucinous ovarian tumors reveals multiple overlapping RAS-pathway activating mutations in borderline and cancerous neoplasms. BMC Cancer 2015;15:415.
[20] Liu SC, Lin H, Huang CC, Chang Chien CC, Tsai CC, Ou YC, et al. Prognostic role of excision repair cross complementing-1 and topoisomerase-1 expression in epithelial ovarian cancer. Taiwan J Obstet Gynecol 2016;55:213–9.
[21] Sung PL, Jan YH, Lin SC, Huang CC, Lin H, Wen KC, et al. Periostin in tumor microenvironment is associated with poor prognosis and platinum resistance in epithelial ovarian carcinoma. Oncotarget 2016;7:4036–47.
[22] Lee WL, Chang WH, Wang KC, Guo CY, Chou YJ, Huang N, et al. The risk of epithelial ovarian cancer of women with endometriosis may be varied greatly if diagnostic criteria are different: a nationwide population-based cohort study. Medicine (Baltimore) 2015;94:e1633.
[23] Wang PH, Sun HD, Lin H, Wang KL, Liou WS, Hung YC, et al. Outcome of patients with recurrent adult-type granulosa cell tumors—a Taiwanese Gynecologic Oncology Group study. Taiwan J Obstet Gynecol 2015;54:253–9.
[24] Wang PH, Lee WL, Juang CM, Yang YH, Lo WH, Lai CR, et al. Altered mRNA expressions of sialyltransferases in ovarian cancers. Gynecol Oncol 2005;99:631–9.